ISSN 1027-4510, Journal of Surface Investigation. X-ray, Synchrotron and Neutron Techniques, 2012, Vol. 6, No. 5, pp. 840–844. © Pleiades Publishing, Ltd., 2012.
Original Russian Text © V.G. Kohn, T.S. Argunova, Jung Ho Je, 2012, published in Poverkhnost'. Rentgenovskie, Sinkhrotronnye i Neitronnye Issledovaniya, 2012, No. 10, pp. 60–65.

On the Cause of a Contrast Change in the SR Images of Micropipes in SiC

V. G. Kohn[a]*, T. S. Argunova[b, c], and Jung Ho Je[c]

[a] *National Research Center Kurchatov Institute, pl. Kurchatova 1, Moscow, 123182 Russia*

** e-mail: kohnvict@yandex.ru*

[b] *Ioffe Physical Technical Institute, Russian Academy of Sciences, ul. Polytekhnicheskaya 26, St.Petersburg, 194021 Russia*

[c] *Pohang University of Science and Technology, Pohang, 790-784, Republic of Korea*

Received January 12, 2012

Abstract—We propose a theoretical explanation for the experimentally observed feature in phase contrast images of micropipes in silicon carbide in a white synchrotron radiation (SR) beam, which consists in the fact that the contrast of various micropipes or various regions of the same micropipe is of different colors. The contrast is most often white (the intensity is higher than the background) at the center and black at the edges; however, the sign sometimes changes, and the contrast becomes black at the center and white at the edges. We discuss the results of experiments performed at the SR source in Pohang, Republic of Korea. The cause of the contrast change can be a change in the angle between the micropipe axis and the SR beam direction. At not overly small angles, the phase progression in a section of the micropipe is small and the contrast is standard. If the angle becomes very small, the size of the longitudinal section of the micropipe by the beam increases, which leads to wave field oscillations in the region of the section. At large distances in the white beam, these oscillations are averaged, and averaging results in black contrast.

DOI: 10.1134/S1027451012100072

INTRODUCTION

Dislocated micro- and nanopipes represent structural defects in silicon carbide (SiC) and gallium nitride (GaN) crystals. The diameters of micropipes in SiC are larger than in GaN by several orders of magnitude; their values are in the range from fractions of a micrometer to ten micrometers. Diagnostics of such defects is an essential part of fabrication, which controls quality, hence, the commercial cost of SiC and GaN substrates. In recent years, the micropipe distribution density in crystalline 4*H*-SiC wafers delivered by the best world manufacturers has not exceeded ~0.7–0.5 cm^2. However, such wafers are very expensive. For the mass production of inexpensive perfect crystals, knowledge of micropipe nucleation and evolution mechanisms, micropipe reactions with each other and with other defects is insufficient. A widely accepted method of micropipe diagnostics in SiC is optical microscopy. However, the resolution and sensitivity of optical micrographs are insufficient for studying the nature of these defects.

The essentials of the nature of micropipes in SiC were obtained by scanning electron microscopy, X-ray topography using synchrotron radiation (SR) [1], and atomic-force microscopy [2]. The simulation of X-ray diffraction patterns measured in white SR allowed determination of the Burgers vectors of dislocations lines along the micropipe axes [1]. In this case, dislocations were assumed to be purely screw type, in strict accordance with the F. Frank theory [3]; the micropipes themselves were assumed to be cylindrical. The results obtained were used by other authors [4]; however, the sizes and morphology of the micropipes themselves have not been independently studied.

Recently, an alternative nondestructive method for studying micropipes, i.e., X-ray phase contrast imaging, has been developed [5–9]. Third-generation SR sources have a small angular size, which provides high spatial beam coherence. Furthermore, the initial SR spectrum, i.e., without monochromatization, is shaped as a curve with a maximum at a certain energy in the case at hand. The decrease in the intensity of the radiation with a high photon energy is caused by the generation mechanism; low-energy radiation is absorbed in the crystal. Therefore, even "white" SR is in part coherent, and this is quite sufficient for recording the phase-contrast images of small objects, such as micropipes in SiC, as bright and dark bands in the central region of the images.

The approach based on imaging in white SR beam is sometimes more preferable in comparison with the use of a monochromator, since a higher intensity determines a short exposure time. The simple experimental setup and the wide wavelength range allow the optimum arrangement of equipment to combine various methods during a single experiment, combining phase-contrast imaging with topography, tomography, and analytical techniques.

However, an analysis of the capabilities of each of the combined methods requires special study. As was first noted in [10], to obtain reliable quantitative data in the phase contrast method, numerical simulation of the images of differently shaped and sized objects should be developed based on the Kirchhoff integral calculation for monochromatic SR harmonics followed by summation over an actual spectrum, taking into account absorption in the sample. Currently, we have developed the FIMTIM program for automatic determination of the parameters of an elliptic micropipe section by the beam, based on fitting the simulated profile of the relative intensity to the experimental one. Using this program, it was shown that during growth the micropipe section can change not only its size, but also its orientation [11, 12].

Further study [13, 14] lead to an understanding of the characteristic feature of the images, which lies in the fact that the image structure weakly depends on the micropipe section's size, especially if the latter is small (less than a micrometer), at relatively long distances (near 50 cm). The size affects only the image contrast, while the image itself has a universal character. An appreciable change in the contrast in experimental images of the micropipe when moving along its axis seemed mysterious for a long time, and this mystery was solved.

In this study, we propose an explanation for another feature of experimental images, i.e., a contrast sign change when moving along the micropipe axis, and opposite contrast signs in images of different tubes. The cause of the contrast sign change is such a change in the micropipe axis direction that it makes a small angle with the SR beam direction. In this case, the size of the micropipe's longitudinal section by the beam increases, which results in strong oscillations of the wave field in the cross section region. At a large distance in the white beam, these oscillations are averaged, which results in black contrast.

We note that micropipes in silicon carbide crystals are interesting objects for studying the general problem of synchrotron phase contrast images, since the transverse diameter of their sections by the beam is comparable to or smaller than the diameter of the first Fresnel zone, and the longitudinal diameter can vary in a wide range. Measurements of experimental images are described in the second section, where examples of contrast changes are also shown. In the third section, the results of a theoretical analysis are presented, which prove the above statement.

EXPERIMENTAL

The 4H-SiC crystal studied in this work was grown by sublimation [15] in an argon atmosphere at a temperature of 2180°C with a rate of 0.5 mm/h. The growth axis was parallel to the [0001] direction. The wafers cut off approximately perpendicular to the growth axis were polished on both sides to a thickness of 0.49 mm. The wafer surface was misoriented with respect to the basal plane by 8°. One of the wafers was then cut into strips 0.5 mm wide, 0.49 mm thick, and 15 mm long.

Phase contrast images were obtained at the 7B2 beamline (X-ray microscopy) of the third-generation Pohang Light Source, Republic of Korea. A bending magnet provided effective source sizes of 60 and 160 μm in the vertical and horizontal directions. The source was at a distance of 34 m from the sample. The effective radiation spectrum was calculated using the source's initial spectrum curve in the energy range from 5 to 40 keV, which is monotonically sloping in shape. After accounting for absorption in a beryllium window 2 mm thick and in the SiC wafer 490 μm thick, the spectrum showed a pronounced maximum at an energy of 16 keV [10]. Radiation that was passed through the sample arrived at a $CdWO_4$ scintillator crystal 200 μm thick and excited its luminescence. Visible light was reflected from a mirror-polished silicon wafer that served as a mirror and passed through a lens system. The magnified image was recorded by a detector with a 1600 × 1200 pixel matrix and a sensitivity of 14 bits. The size of the field of view was 540 μm (H); the pixel size was 0.34 μm.

The samples were fixed on a holder providing movement along three axes with an accuracy of 0.1 μm, tilts and rotation about the vertical axis. The sample surface was aligned perpendicular to the beam; in this case, the micropipe axes were perpendicular to the basal plane, deviating from the normal to the surface by 8°. The distance between the scintillator and the sample was varied from 5 to 30 cm. The phase contrast images were measured in two modes: (i) by translation and (ii) by rotation of the samples in the form of bars about the vertical axis perpendicular to the beam and parallel to the long edge of the bar. In the former mode, the micropipe distribution in the sample bulk was determined; in the latter mode, the micropipe orientation in space was studied. The rotation was performed in the range of 180° with a step of 2°. The imaging was performed step-by-step in the fast-shutter shooting mode.

Figure 1 shows the typical phase contrast images of the series measured by sample rotation in the SR beam. When the longitudinal-cut surface of the bar is illuminated, micropipes are seen over the entire length (not shown in the figure). In some places, they deviate from the growth axis by significantly larger angles than the misorientation angle of 8°. We can see contrast sign changes along the micropipe axes. The typical contrast (dark edges and bright center) changes to the reverse one (black center and bright edges). The change is caused by the micropipe axis rotation angle with respect to the beam direction.

THEORY

Phase contrast images of the micropipes in the white SR beam can be theoretically calculated as an

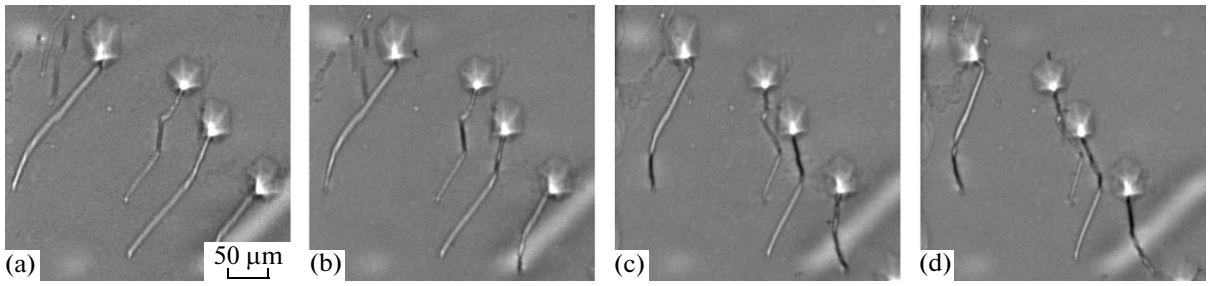

Fig. 1. Representative phase contrast images of micropipes in a silicon carbide sample among the sequences of the images registered while rotating the sample in a SR beam. Adjacent panels in the series from (a) to (d) differ in sample rotation angle by 2°. We can see the contrast sign variation along the micropipe axes with sample orientation with respect to the beam axis.

incoherent superposition of images for various harmonics, where the weight of each harmonic (effective radiation spectrum) should be calculated taking into account its intensity absorption in the path from the source to the detector. We note that consideration of absorption in a relatively thick sample can cause a significant change in the effective spectrum. For example, for the Pohang Light Source, the spectrum has a maximum at the photon energy $E = 16$ keV and sharply decreases with decreasing energy, i.e., even in the absence of a monochromator, the actual spectrum forming the image is localized near 16 keV. Such a spectrum depends on the source and the thickness of all absorbers in the beam path. A slight shift in the maximum can be achieved by varying the absorber thickness; however, the energy cannot be varied in a wide range.

The monochromatic image of the micropipe can be calculated in the approximation of a quasi-linear object which strongly changes the phase of the wave passing through it across the axis and very weakly changes it along the axis. Separating the relative intensity profile $I(x)$ in any section across the axis, we can disregard the phase change along the axis. In this approximation, the intensity profile is described using the single integral in infinite limits,

$$I(x) = |a(x_0)|^2, \quad a(x_0) = \int dx_1 P_K(x_0 - x_1, Z) T(x_1), \qquad x_0 = x\frac{z_0}{z_t}, \tag{1}$$

where z_0 is the source–object distance, z_1 is the object–detector distance, $z_t = z_0 + z_1$, $Z = z_0 z_1 / z_t$. In this case, the problem is reduced to the calculation of the convolution of two functions, the first of which is the Kirchhoff propagator

$$P_K(x, z) = \frac{1}{(i\lambda z)^{1/2}} \exp\left(i\pi \frac{x^2}{\lambda z}\right), \tag{2}$$

where λ is the radiation wavelength. The second function $T(x)$ is called the transmission function. It describes the influence of the object on the coherent wave. For small objects, it is sufficient to consider the change in the phase and amplitude of the wave within geometrical optics without changing the ray trajectories, i.e., assuming that all rays are parallel to the optical axis. For a void that has an elliptical cross section in a material, only wave distortion due to inhomogeneity should be taken into account. As a result, we have $T(x) = 1$ at $|x| > R$; at $|x| < R$,

$$T(x) = \exp\left[(iP + M)\left(1 - \frac{x^2}{R^2}\right)^{1/2}\right], \quad P = \frac{4\pi}{\lambda}\delta R_0, \qquad M = P\frac{\beta}{\delta}. \tag{3}$$

Here $2R$ and $2R_0$ are the diameters of the elliptical cross section of the micropipe across and along the beam, respectively, $\delta - i\beta = 1 - n$, where n is the complex refractive index of the medium. In the experiment, the diameters of the elliptical cross section are a priori unknown and should be determined.

Since the integrand in (1) does not decay at infinity, for numerical calculations, the integral should be rewritten in the form

$$a(x_0) = 1 + \int dx_1 P_K(x_0 - x_1, Z)[T(x_1) - 1], \tag{4}$$

using the known propagator normalization property. The intensity profiles for monochromatic harmonics were calculated in the point grid in the range from 5 to 40 keV and then were summed taking into account the spectrum given in [10–12]. Numerical simulation of the images was performed using the FIMTIM program described in [11–12].

To better understand the physics of the formation of coherent monochromatic images, we will simplify the problem making evident approximations. First, we can neglect absorption and write $M = 0$. Since $z_0 \gg z_1$, we can turn to the plane-wave approximation ($z_0 = \infty$) and replace x_0 with x and Z by z_1. We also note that the Kirchhoff propagator weakly varies at transverse distances shorter than the radius of the first Fresnel zone $r_1 = (\lambda z_1)^{1/2}$. For $E = 16$ keV and at the distance $z_1 = 30$ cm, we have $r_1 = 4.8$ μm. The transverse diameter of almost all micropipes is $2R < r_1$. This means that we

can disregard the term $\pi(x_1/r_1)^2$ in the propagator phase in calculating the integral, which is exactly the Fraunhofer diffraction approximation.

Taking into account these approximations, we obtain the following expressions for function (4)

$$a(x) = 1 + \frac{2R}{i^{1/2} r_1} \exp\left(i\pi \frac{x^2}{r_1^2} \right) B(x), \quad (5)$$

$$B(x) = \frac{1}{2} \int_{-1}^{1} dt \exp\left(-i \frac{x}{x_0} t \right) \left[\exp\left(iP\left(1 - t^2\right)^{1/2} \right) - 1 \right], \quad (6)$$

$$x_0 = \frac{r_1^2}{2\pi R}.$$

The case where $P \ll 1$ was considered in [13, 14]. In this case, the bracketed exponent in the integrand in formula (6) can be expanded in a power series and the analysis can be restricted to the first expansion term. Then we find that the characteristic size of the central region is $2r_1$, and the contrast of this region is bright, i.e., the relative intensity at the center is larger than unity.

It is easy to understand that, when the parameter $s = 2R/r_1 \ll 1$, the central region's size is defined by the universal exponent in formula (5), and the function $B(x)$ weakly depends on its argument in this region at all values of P, since $x_0 > r_1$. However, it is clear that the contrast sign depends on P. At the same time, we have the following formula $P = P_0/\sin\alpha$, where α is the angle between the micropipe axis and the SR beam direction, and P_0 is the value of P in the case of perpendicular orientation. Even if $P_0 \ll 1$, the reverse situation can be obtained, i.e., $P \gg 1$, as the angle α decreases. Let us consider the relative intensity $I(0) = |a(0)|^2$ at the image center as a function of the parameter P at various values of parameter s. The analytical expression for integral (6) has a complex form and is inapplicable for analysis.

Figure 2 shows the dependences of $I(0)$ on P, numerically calculated for $s = 0.3$, 0.6, and 0.9. As follows from the calculated results, at small P no larger than unity, the image at the center exhibits bright contrast which is proportional to both P and s. This result was analytically obtained in [13, 14]. However, as the parameter P is further increased, the intensity at the center reaches a maximum and then decreases to negative values. In other words, the contrast sign changes from bright to dark. It is noteworthy that the dependence is oscillatory, i.e., the dark contrast again transforms to bright and vice versa as P increases.

To compare the calculated monochromatic images with the images obtained in experiments with a white SR beam, it is necessary to sum the curves corresponding to different wavelengths, taking into account the actual radiation spectrum. Since the parameter P depends linearly on λ (see (3), where $\delta \propto \lambda^2$), at large values of P and taking into account the large width of the radiation spectrum from the bending magnet, it is impossible to detect contrast oscillations in the dependence of the tilt angle α; if the latter is small, the contrast is always black. This result follows from the FIMTIM calculations illustrated in Fig. 3, where the intensity profiles for the micropipe with a round section 3 μm in diameter at a distance of 30 cm from the sample are shown. All other parameters for the SR source in Pohang are standard: the effective source size is 60 μm, the source–sample distance is 34 cm, and the SiC wafer sample thickness is 490 μm.

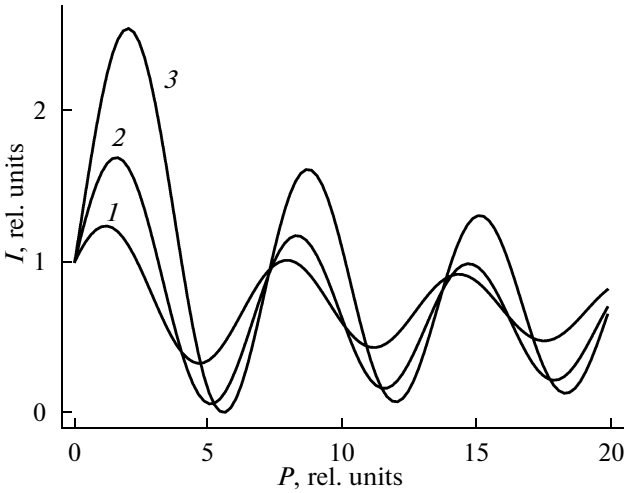

Fig. 2. Dependence of the relative intensity of monochromatic radiation at the image center on the dimensionless parameter P at various values of the parameter s, equal to 0.3 (curve *1*), 0.6 (curve *2*), and 0.9 (curve *3*). The calculation is performed by formulas (5) and (6) at $x = 0$.

Figure 3 shows six curves at various tilt angles of the micropipe axis to the SR beam direction. These values (in degrees) are shown in plots. The first curve corresponds to the perpendicular orientation. In this case, the contrast is relatively weak, and the intensity at the center is higher than the background: the image is bright. As the tilt angle decreases, the contrast initially increases retaining its shape; then, the intensity at the center gradually decreases, the contrast becomes dark; at very small tilt angles, the contrast decreases again.

CONCLUSIONS

Phase contrast images of micropipes in silicon carbide change contrast sign when the sample is rotated in a SR beam. The cause of this effect is such a change in the micropipe axis direction that it makes a small angle with the beam direction. In this case, the size of the longitudinal micropipe section by the beam increases. When using monochromatic radiation, the dependence is oscillatory. In white SR, the summation of curves corresponding to different wavelengths λ, taking into account the actual radiation spectrum, leads

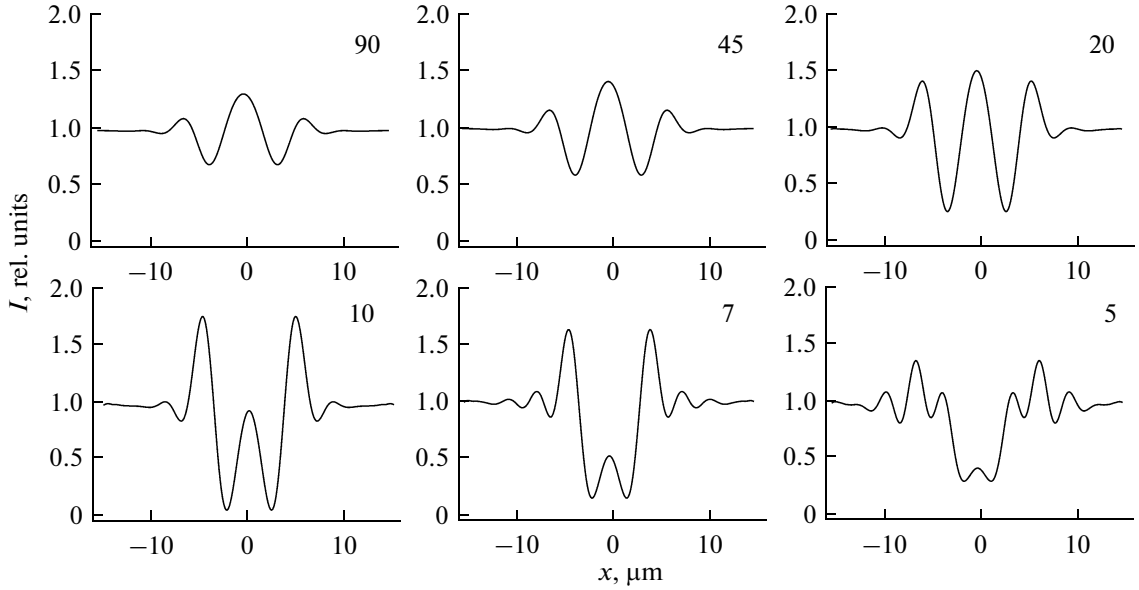

Fig. 3. Dependences of the relative intensity of a white SR beam on the transverse coordinate x for various angles between the micropipe axis and the SR beam direction. The angles in degrees are indicated in the panels. The calculation was performed by the FIMTIM program for typical values of parameters corresponding to the experimental conditions.

to averaging of the oscillations, and the resulting contrast is always black.

The effect determined and described in this study does not prevent the study of microscopic object morphology in white SR. Knowing the cause, a sample can be prepared and an experiment can be performed so that the contrast change would not complicate the reconstruction of three-dimensional tomographic images.

The simulation of images confirms the conclusions of the theory of defects about the reactions of micropipes in regions of their dense groups. Entering into the reactions, micropipes move parallel to the growth front toward each other and to other defects. The estimates of the tilt angles at which the black contrast appears do not contradict micropipe deviations from the growth axis, caused by the reactions [6–9].

ACKNOWLEDGMENTS

This study was supported by the Russian Foundation for Basic Research, project no. 10-02-00047a and Creative Research Initiatives (Functional X-ray Imaging) of MEST/KOSEF of Korea.

REFERENCES

1. X. R. Huang, M. Dudley, W. M. Vetter, et al., Appl. Phys. Lett. **74**, 353 (1999).
2. J. Heindl, W. Dorsch, H. P. Strunk, et al., Phys. Rev. Lett. **80**, 740 (1998).
3. F. C. Frank, Acta Crystallogr. **4**, 497 (1951).
4. I. Kamata, H. Tsuchida, T. Jikimoto, et al., Jpn. J. Appl. Phys. Pt. 1 **39**, 6496 (2000).
5. T. S. Argunova, M. Yu. Gutkin, J. H. Je, et al., J. Mater. Res. **17**, 2705 (2002).
6. M. Yu. Gutkin, A. G. Sheinerman, T. S. Argunova, et al., J. Appl. Phys. **100**, 093518 (2006).
7. M. Yu. Gutkin, A. G. Sheinerman, T. S. Argunova, et al., Phys. Rev. B **76**, 064117 (2007).
8. M. Yu. Gutkin, A. G. Sheinerman, M. A. Smirnov, et al., Appl. Phys. Lett. **93**, 151905 (2008).
9. M. Yu. Gutkin, A. G. Sheinerman, and T. S. Argunova, Phys. Status Solidi C **6**, 1942 (2009).
10. V. G. Kohn, T. S. Argunova, and J.-H. Je, Appl. Phys. Lett. **91**, 171901 (2007).
11. T. S. Argunova, V. G. Kohn, and J.-H. Je, J. Surf. Invest. **2**, 861 (2008).
12. T. Argunova, V. Kohn, J-W. Jung, and J.-H. Je, Phys. Status Solidi A **206**, 1833 (2009).
13. V. G. Kohn, T. S. Argunova, and J.-H. Je, J. Phys. D: Appl. Phys. **43**, 442002 (2010).
14. V. G. Kohn, T. S. Argunova, and J.-H. Je, J. Surf. Invest. **5**, 1 (2011).